A volumetric census of the Barents Sea in a changing climate

Sylvain Watelet[1,4], Øystein Skagseth[2], Vidar S. Lien[2], Helge Sagen[2], Øivind Østensen[2], Viktor Ivshin[3], and Jean-Marie Beckers[4]

[1]Observation Scientific Service, Royal Meteorological Institute, Brussels, Belgium [current affiliation]
[2]Institute of Marine Research, Bergen, Norway
[3]Polar Branch of Russian Federal Research Institute of Fisheries and Oceanography (PINRO), Murmansk, Russia
[4]Department of Astrophysics, Geophysics and Oceanography, GeoHydrodynamics and Environment Research Unit, FOCUS Research Unit, University of Liège, Liège, Belgium

Correspondence: Sylvain Watelet (swatelet@uliege.be)

Abstract.

Due to its location between the Norwegian Sea and the Arctic Ocean, the Barents Sea is one of the main pathways of the Atlantic Meridional Overturning Circulation. Changes in its water masses potentially affect the thermohaline circulation through the alteration of the dense water formation process. In order to prospect such changes, we present here a seasonal atlas of the

5   Barents Sea including both temperature and salinity for the period 1965–2016. The atlas is built as a compilation of datasets from the World Ocean Database, the Polar Branch of Russian Federal Research Institute of Fisheries and Oceanography, and the Norwegian Polar Institute using the Data-Interpolating Variational Analysis (DIVA) tool. DIVA allows for a minimization of the expected error with respect to the true field. The atlas is used to provide a volumetric analysis of water mass characteristics and an estimation of the ocean heat and freshwater contents. The results show a recent "Atlantification" of the Barents Sea, i.e.

10   a general increase of both temperature and salinity, while its density remains stable. The atlas is made freely accessible as user-friendly NetCDF files to encourage further research in the Barents Sea physics (https://doi.org/10.21335/NMDC-2058021735, Watelet et al. (2020)).

1 Introduction

15   The Barents Sea shelf is a "hotspot" in the ongoing, rapid climatic changes taking place in the Arctic (Lind et al., 2018). During recent decades, the Barents Sea has (BS) contributed the most to the reduction in Arctic winter sea-ice cover (Yang et al., 2016). Moreover, the northern, Arctic–dominated part of the Barents Sea has experienced an Atlantification (or "borealization") with profound impact on both physical conditions, such as water mass transformations and properties (Lind et al., 2018), as well as biology and marine ecosystem (Fossheim et al., 2015). As the northern limb of the Atlantic Meridional Overturning Circulation

20   (AMOC) and a source for dense Arctic Intermediate Water (Schauer et al., 1997), changes to the water mass transformation
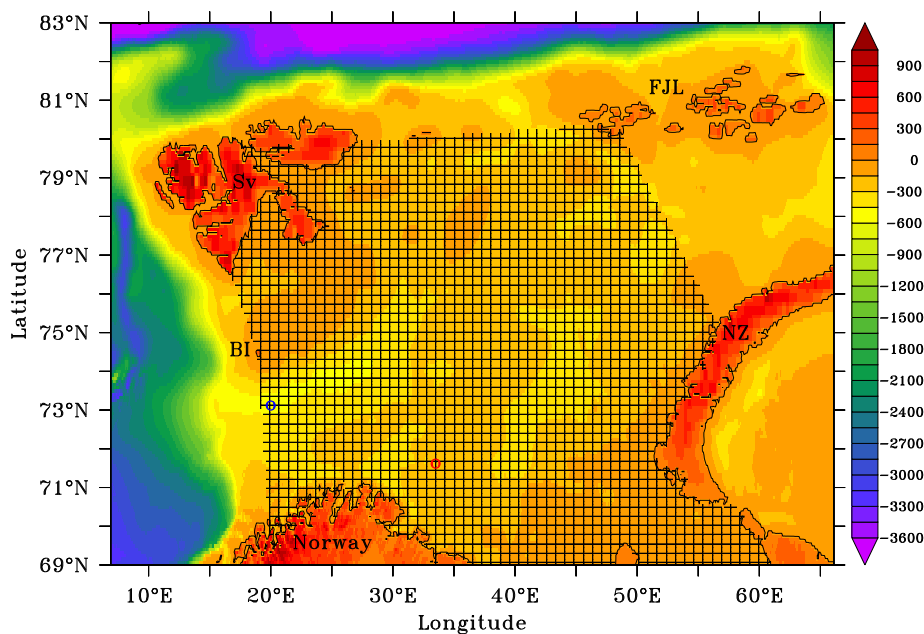
Figure 1. Bathymetry of the BS and its neighbouring seas. Our analyses on the Barents Sea correspond to the shaded region. The Barents Sea Opening, located between the Norwegian coast and Bear Island, and the Kola sections are shown as blue and red circles respectively. BI stands for Bear Island, Sv for Svalbard, FJL for Franz Jozef Land and NZ for Novaja Zemlja.

processes in the Barents Sea affect the thermohaline circulation of the North Atlantic and Arctic oceans (Swift et al., 1983; Kuhlbrodt et al., 2009; Mauritzen et al., 2013; Lozier et al., 2019).

The Barents Sea is the largest shelf sea of the Arctic Ocean, and it is bounded by Norway and the Kola Peninsula (Russia) to the south, the Svalbard and Franz Josef Land archipelagos to the north, and Novaya Zemlya to the east (see Fig. 1). The
25 Barents Sea is connected to the Norwegian Sea to the west through the Barents Sea Opening (BSO), and to the Arctic Ocean to the north and northeast. Together with the Fram Strait between Svalbard and Greenland, the BSO is the main gateway between the North Atlantic and the Arctic and, thus, a main pathway for Atlantic Water transport northwards from the Nordic Seas to the Arctic Ocean (Knipowitsch, 1905; Helland-Hansen and Nansen, 1909). Due to its climatic importance and vast marine resources, the Barents Sea area is sampled and monitored on a seasonal timescale (Eriksen et al., 2018). However, the coverage
30 may vary between seasons and years, and especially for the winter and spring seasons, and the spatial coverage is sometimes only semi-synoptic or concentrated in fixed sections.

Satellite remote sensing provides observations of surface temperature, and recently also salinity, with high resolution in both space and time. E.g., using AVHRR data, Comiso and Hall (2014) found the northern Barents Sea to be one of the areas within the Arctic with the highest temperature increase in the period 1981–2012. Furthermore, they found a significant decline in
35 sea-ice cover between the two periods 1979–1995 and 1996–2012. However, to investigate regional climate processes, such as water mass transformation and properties changes, in-situ observations are needed. In situ data often has the disadvantages of

a limited coverage in space (e.g. hydrographic sections) or time (e.g. ship surveys). Thus, when investigating changes in space and time, observations provided on a regular grid are desirable.

Here, we present a gridded dataset of temperature and salinity in the Barents Sea region at seasonal temporal resolution for
40 the period 1965–2016, based on all available observations. The dataset is compiled using the Data-Interpolating Variational Analysis (DIVA) tool. We provide the dataset including fields of expected error, and present two examples of usage where this gridded dataset has an advantage over the non–gridded raw data: volumetric analysis of water mass characteristics, and estimation of ocean heat and freshwater content.

2   Data sources

45 Non–gridded and non–interpolated in–situ hydrographic data were obtained from World Ocean Database 2013 (WOD13) including data through 2016, although with more limited data quality control for the years post 2013. The WOD13 data were limited to the area between 7–66°E and 68–83°N. In addition, we have included Conductivity–Temperature–Depth (CTD) data from the Polar Branch of Russian Federal Research Institute of Fisheries and Oceanography (PINRO) for the period 1965–2014, and from the Norwegian Polar Institute (NPI) for the years 1998, 2003, 2004, 2005, and 2011.

3   Software and method

Ocean Data View (ODV) software was used to convert the hydrographic data sets into a format readable by the DIVA software: the ODV spreadsheet (https://www.bodc.ac.uk/resources/delivery_formats/odv_format/).

DIVA is a statistical software designed to generate continuous fields from heterogeneously distributed in situ data by making use of a Variational Inverse Method (Brasseur, 1995; Troupin et al., 2012). The result of its variational analysis are gridded
55 fields which minimise the expected errors with respect to the unknown true fields. Under a few assumptions on the correlations, the Variational Inverse Method is equivalent to the popular Optimal Interpolation (Rixen et al., 2000).

Using DIVA preprocessing tools, the ODV spreadsheets were vertically interpolated onto 23 depths (500, 450, 400, 350, 300, 250, 200, 175, 150, 125, 100, 75, 50, 45, 40, 35, 30, 25, 20, 15, 10, 5, 0) following the Weighted Parabolas method (Reiniger and Ross, 1968). These levels were chosen in view of increasing the resolution next to the surface where the variability of both
60 temperature and salinity are expected to be higher.

The BS bathymetry was extracted from the General Bathymetric Charts of the Oceans (GEBCO) at a spatial resolution of 30 seconds by using Diva-on-web (http://ec.oceanbrowser.net/emodnet/diva.html). This bathymetry was then downgraded to a resolution of 1/8x1/8° in order to avoid too complex shapes when computing the coastlines for each depth level. All data falling outside these coastlines or outside the full domain (6.9–66.1°E ; 69–83°N) shown in Fig. 1 were removed. The remaining data
65 availability is shown in Fig. 2 for temperature and in Fig. 3 for salinity.

For each of the 23 layers and for each year between 1965–2016, the objective is to perform analyses on four seasons : November to January, February to April, May to July and August to October. Before generating these analyses, we had to
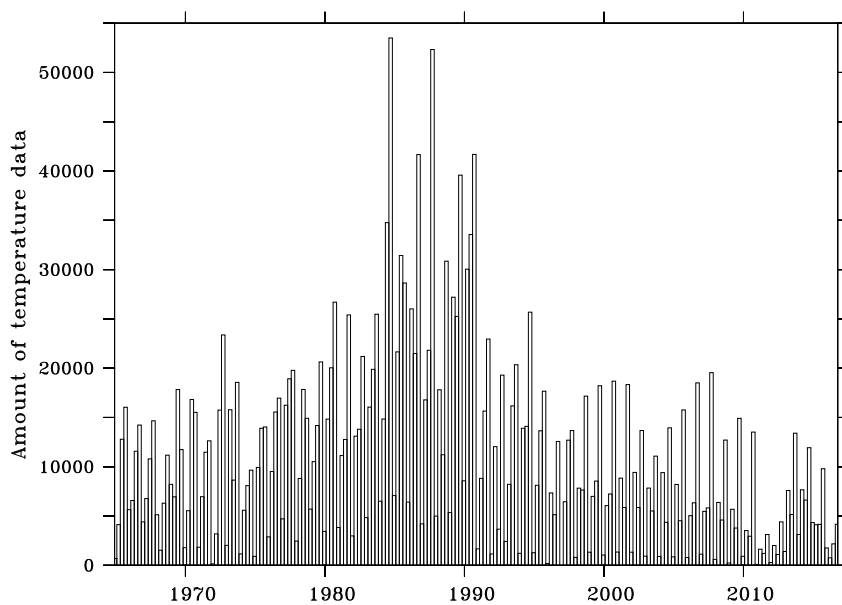
Figure 2. Availability of temperature data in the Barents Sea as a function of time.
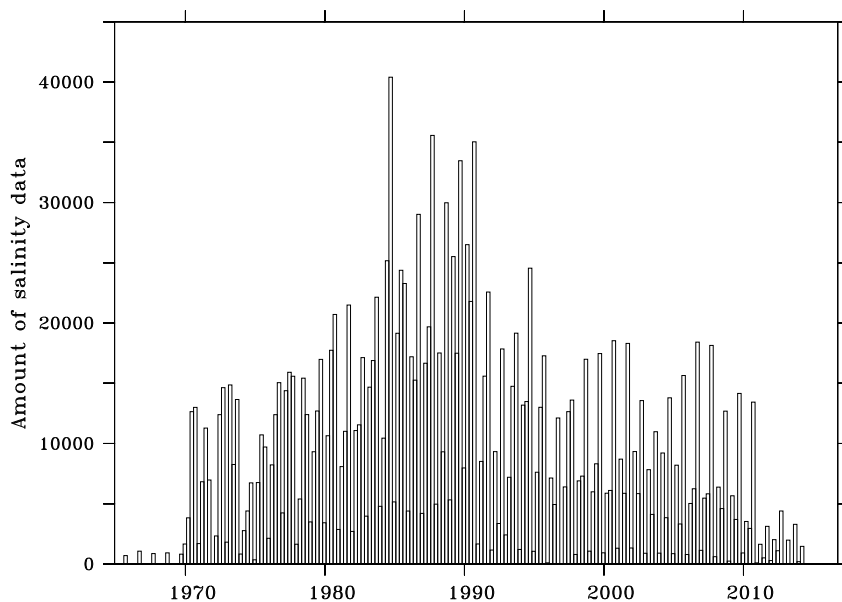
Figure 3. Availability of salinity data in the Barents Sea as a function of time.

choose a reference field, namely a first guess state, for each analysis. By subtracting this reference field from the original data, DIVA directly works with anomalies of temperature and salinity before adding back the reference to the optimal analysis.
70   In this way, the analysis tends to smoothly reach the reference values in the absence of data. The first step to generate these reference fields is the collection of all the temperature or salinity data across several years surrounding the year to be analysed, for each season. A running window of 11 years centered at the year of interest is used, except near the beginning and end of the period where the window size is reduced to the available years. These 208 reference fields, each made of 23 layers, are generated by performing a first analysis using the simple data average for each layer as a very first guess.

75   From there, the correlation length is estimated by a fit between the empirical data correlation function as a function of the distance and its theoretical counterpart, while the signal to noise ratio is approximated by cross validation techniques (Craven and Wahba, 1978). Both parameters are thus estimated on the basis of the data sets. The correlation length and the signal to noise ratio are both filtered vertically to avoid unrealistic discontinuities between depth levels, and the latter is capped at 10 to avoid an overconfidence in the data accuracy. Using these statistical parameters, the reference fields are computed by the
80   Variational Inverse Method with DIVA over the same 11 years, for each season.

Then, all the seasonal analyses between 1965–2016 are performed on a yearly basis, using the corresponding 11 years reference fields and the same statistical parameters. Indeed, we decided to use those parameters based on a larger amount of data (11 years) in order to increase their robustness and decrease their variability. The analyses are stored on a 0.1x0.1° output grid. In order to assess the reliability of the analyses, an error field associated with each of them is computed by using the clever
85   poor man's method, a good compromise between the computation time and the accuracy (see Beckers et al. (2014)). This error field on the analysis is then compared to the error on the first guess, namely the relative error field which thus consists in a score comprised between 0 and 1. Qualitatively, this score measures the added value brought by in situ data to the analysis: 0 would be the true field while 1 corresponds to an absence of data, i.e. an analysis equal to the first guess.

4   Temperature and salinity Atlas

90   The temperature and salinity atlas is available at the Norwegian Marine Data Centre as two NetCDF files. Each file contains analyses of temperature or salinity, respectively, for all seasons and years at all depths, and also includes the error field associated with each analysis. The statistical parameters and the analysed fields masked when the relative error exceeds 0.3 or 0.5 are also available to enable a quick visualisation of the most reliable areas. The data is accessible at https://doi.org/10.21335/NMDC-2058021735 (Watelet et al., 2020).

5   Temperature and Salinity changes between 1994–1998 and 2006–2010

Lind et al. (2018) gave some evidence suggesting a warmer and saltier northern BS from mid–2000s than previously. This Section aims at examining the case for the whole BS between 1994–1998 and 2006–2010 by using volumetric Temperature–Salinity (*T-S*) diagrams.
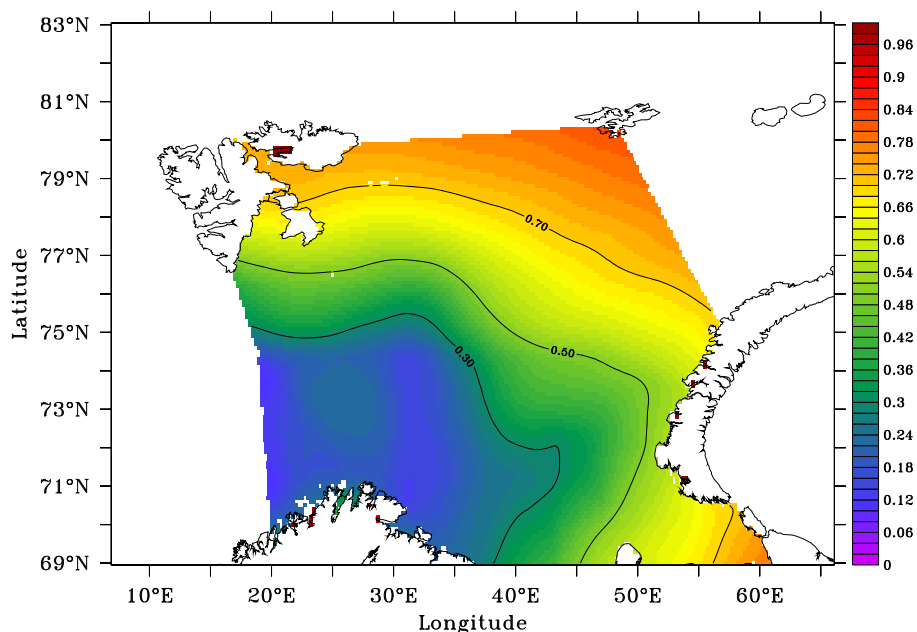
Figure 4. Average relative error at the Barents Sea surface for temperature between 1965–2015.

First of all, the uncertainties on the Atlas have to be considered. The BS has a varying data coverage depending on years,
100 seasons but also sub-regions. Fig. 4 and 5 show the average relative error fields between 1965–2015 at the BS surface. The
geographical pattern of these error fields are similar at other depths (not shown). The errors are much higher in the northern
and eastern parts of the BS than in the western and southern parts (see Section 6). The relative error field averaged on all layers
for each season is shown for each variable in Fig. 6a and Fig. 6b. For both variables, the uncertainty is minimum in the 1980s
and during autumns, when the number of measurements is highest (Figs. 2, 3). For this reason, we decided to focus on the
105 autumn only when considering the whole BS.

Volumetric *T-S* diagrams for both 1994–1998 and 2006–2010 were then carried out by summing all pixels falling inside
T-S classes defined by temperature ranging from -1 to 7 °C and salinity varying between 33 and 35.5 PSU by step of 0.05
°C and 0.025 PSU, respectively. Beforehand, each pixel is given the value of the vertical extent of the corresponding layer, in
order to get a final result more proportional to the water volume of each *T-S* class. Since we use no horizontal weighting, the
110 narrowing of the longitudinal bands towards the north is here not taken into account. For example, the area of the southernmost
pixel at 69°N is $4.4 \times 10^7 \, \mathrm{m}^2$ while the northernmost pixel at 80°N is $2.1 \times 10^7 \, \mathrm{m}^2$. The average of both periods is shown in
Fig. 7a. Finally, the difference between 2006–2010 and 1994–1998 diagrams is shown in Fig. 7b. On this Figure, the increase
in temperature and salinity is clear, while the density remains more or less unchanged due to the cancelling effects from the
increasing haline contraction and thermal expansion on density.

115 In addition to the choice of the most reliable season and the use of 10-year seasonal reference fields in order to mitigate the
errors at most, we provide an estimation of the uncertainties for both 5-year periods used above. In Fig. 7c and 7d, the average
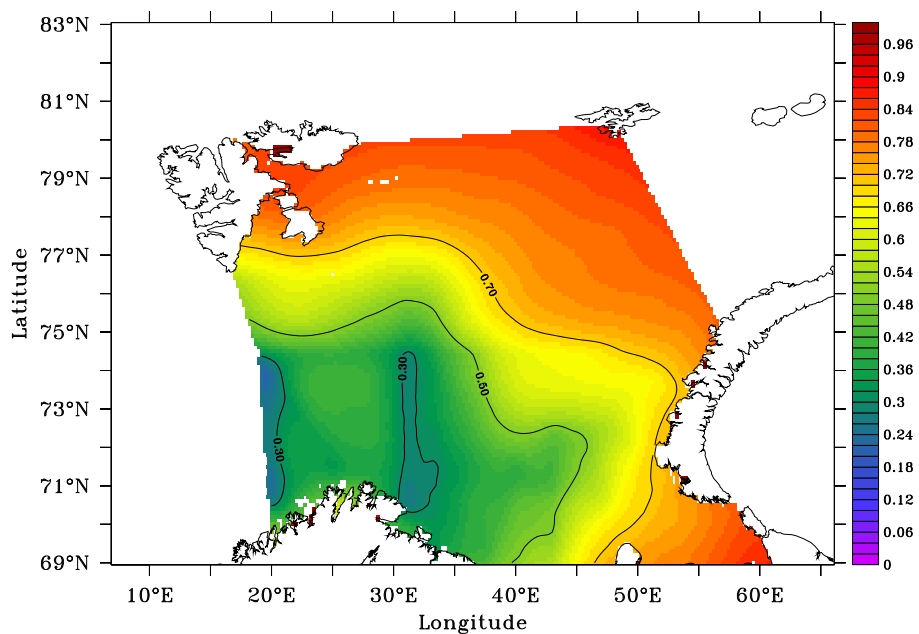
Figure 5. Average relative error at the Barents Sea surface for salinity between 1965–2015.
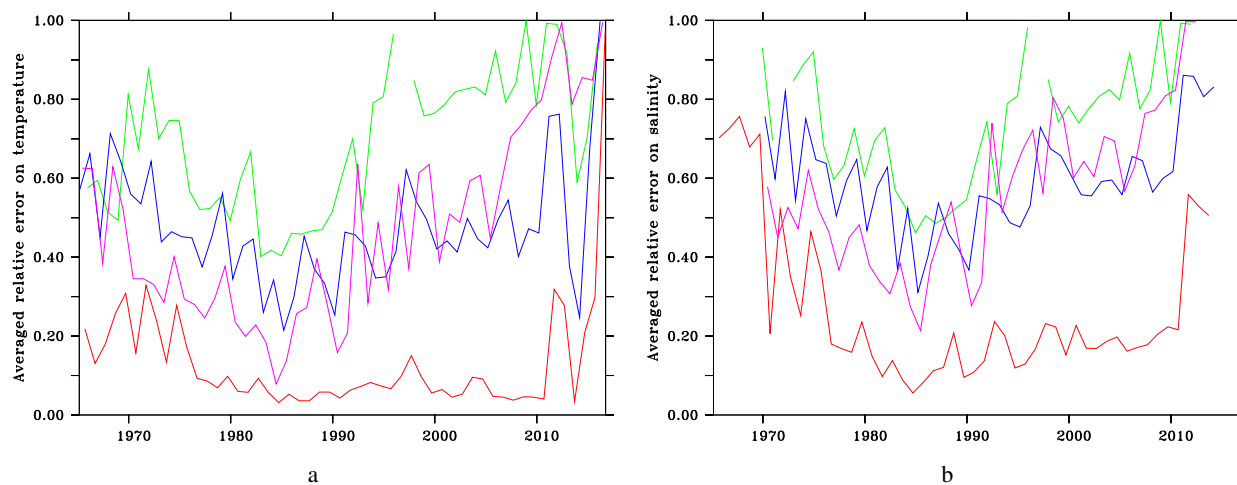
Figure 6. (a) Average relative error on the Barents Sea for temperature as a function of seasons: autumn (red), winter (green), spring (blue), summer (purple). (b) Average relative error on the Barents Sea for salinity.
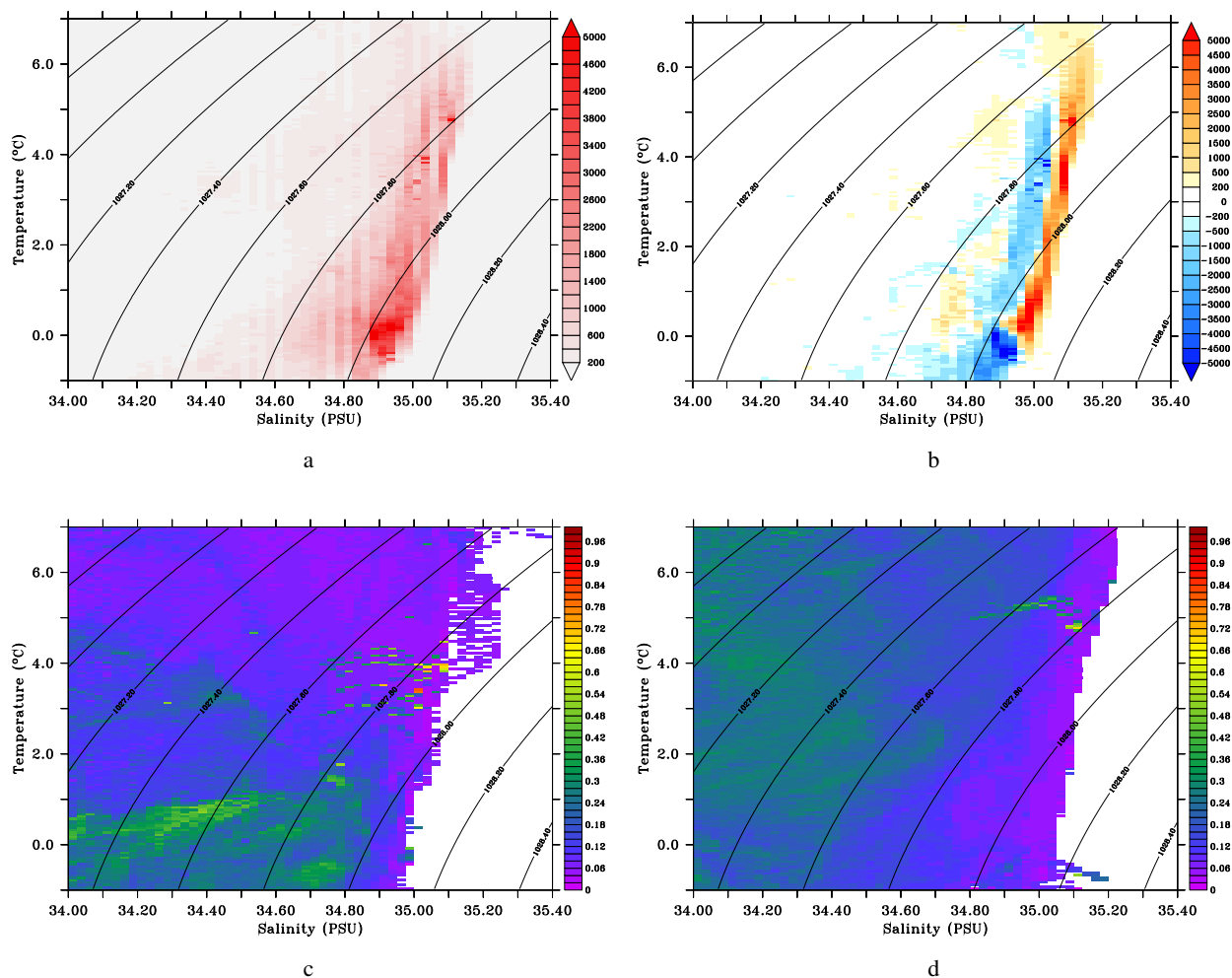
Figure 7. (a) Average volumetric *T-S* diagrams during 1994–1998 and 2006–2010. A value of 1 corresponds to a pixel with a vertical extent of 1 m. Isopycnals are shown for 0 m (black). (b) Difference in volumetric *T-S* diagrams between 2006–2010 and 1994–1998. (c) Average relative error weighted by the layer thickness for each *T-S* class between 1994–1998. (d) Average relative error weighted by the layer thickness for each *T-S* class between 2006–2010.

relative error weighted by layer thickness is shown for each *T-S* class for 1994–1998 and 2006–2010, respectively. Comparing both Figures to Fig. 7b and *T-S* diagrams of both periods (Fig. 7a), it is clear the error is much lower on *T-S* classes experiencing large changes, which are also the most represented classes by far. This strengthens the reliability of the observed *T-S* changes.
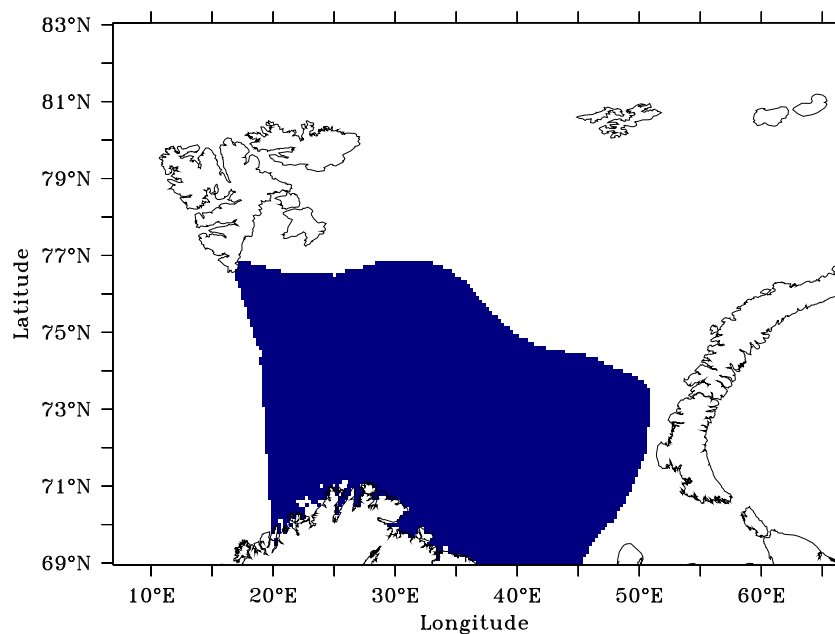
Figure 8. Most reliable area as defined from temperature and salinity relative errors.

6 Most reliable area

6.1 Uncertainties

In this Section, we focus for two reasons on the dark blue sub-region on Fig. 8 hereafter referred to as the Most Reliable Area (MRA). First, the MRA comprises the southern part of the BS dominated by the Atlantic Water throughflow. Second, this is the most observed sub-region for both temperature and salinity as highlighted by the error estimates in Fig. 4 and 5. Similarly to the whole BS, relative error fields are averaged by season (see Supplementary Material). Compared to the BS, the MRA shows relatively low uncertainties for all seasons due to much better data coverage, even if the autumn remains the most reliable and the winter the least. This advantage allows us to work with all seasons in the MRA, in contrast to the whole BS, provided we focus on shortened periods: 1965–2015 for temperature and 1970–2010 for salinity. Within these periods, the 1996–1997 winter temperature and the 1971–1972 winter temperature and salinity are not analysed due to the lack of data.

6.2 Temperature, salinity and density profiles

One way of studying changes in temperature and salinity in the MRA is to look at the vertical dimension. Temporal evolution of seasonally averaged profiles of both temperature and salinity are shown in Fig. 9 and 10. Between 1965–2015, the temperature gradually increased throughout the whole water column. Considering salinity, matters are not so clear, except the unambiguous raise between the 90s and the 2000s, similarly to the observation made for the whole BS. The potential density relative to the
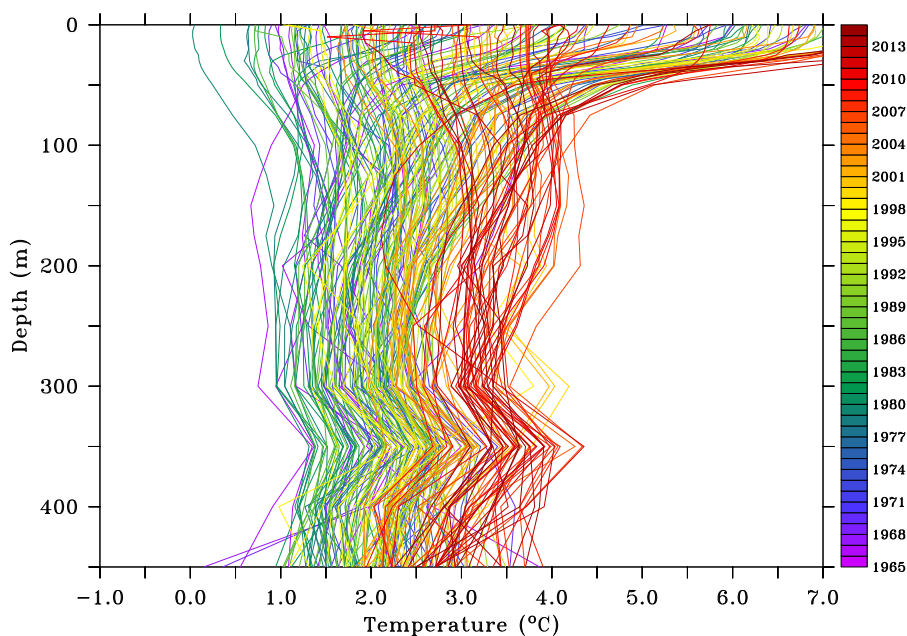
Figure 9. Seasonal averaged profiles of temperature on the Most Reliable Area between 1965–2015.

surface is shown in Fig. 11. There is no clear trend throughout the period, which might indicate the observed warming trend is compensated to some extent by a salinity increase.

6.3 Volumetric changes in temperature, salinity and density

Further analyses of volumetric changes in the MRA are performed in order to better assess the evolution of temperature, salinity and density classes throughout the water column. These calculations are performed for each season between 1965–2015 for temperature and between 1970–2010 for both salinity and density. Fig. 12 shows the evolution of temperature classes ranging from -1 to +7 °C. There is a clear increase in the volume of the warmest temperature classes at the expense of the coldest classes throughout the period. Changes in salinity classes between 34.4 and 35.2 PSU are shown in Fig. 13. Here, matters are less clear but there is however an increase of salinity classes above 35 PSU and a decrease of the lowest-salinity class between 1980–2010. Finally, the potential density relative to the surface is used in Fig. 14 where classes range between 1027.2 and 1028.8 $kg.m^{-3}$. The potential density does not display large changes on the long term, similarly to Section 6.2.

6.4 Ocean Heat Content

The Ocean Heat Content (OHC) of the MRA is calculated following the method described in Boyer et al. (2007):

$$OHC = \iiint \rho(t,s,p)c_p(t,s,p)\Delta t\,dxdydz \tag{1}$$
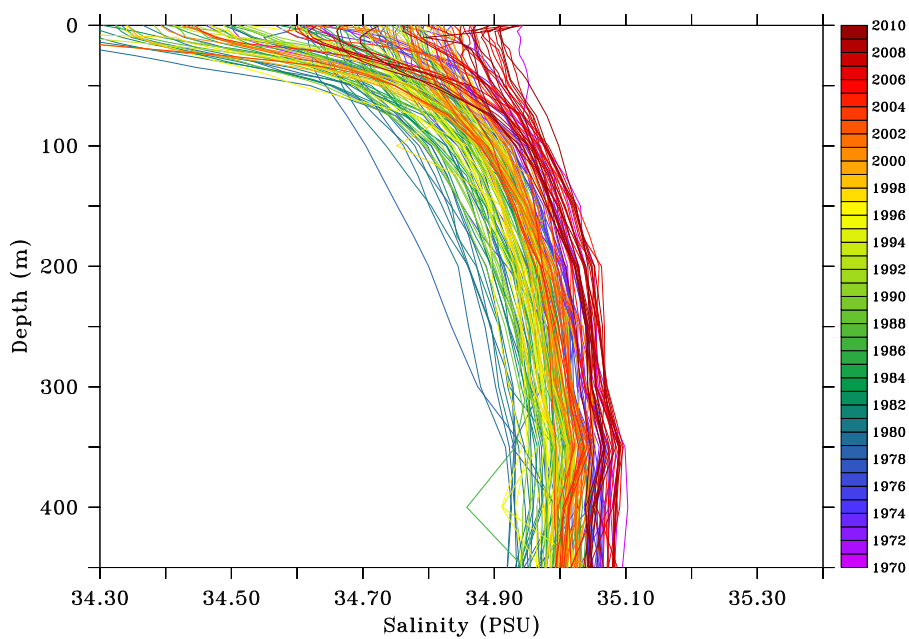
Figure 10. Seasonal averaged profiles of salinity on the Most Reliable Area between 1970–2010.
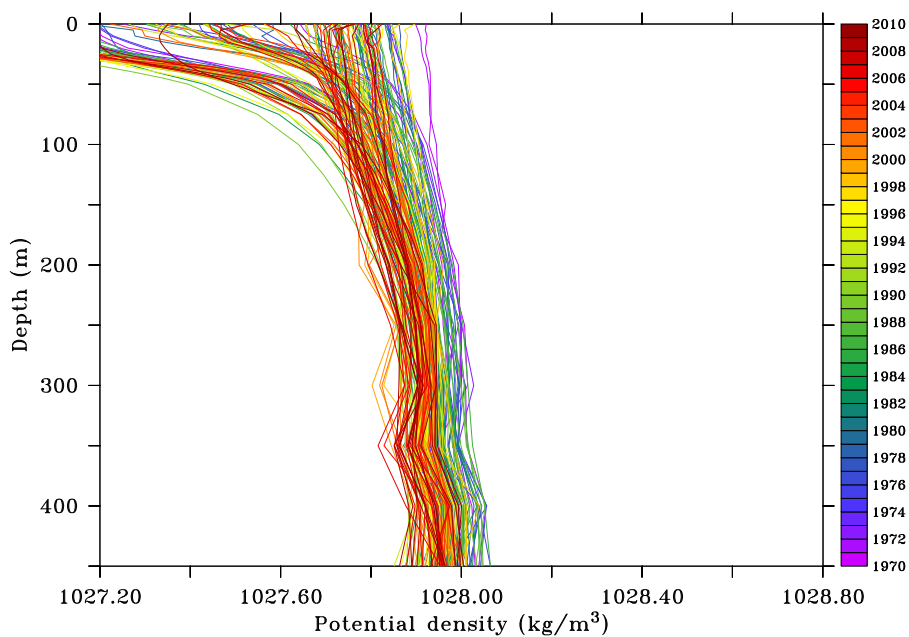
Figure 11. Seasonal averaged profiles of potential density on the Most Reliable Area between 1970–2010.
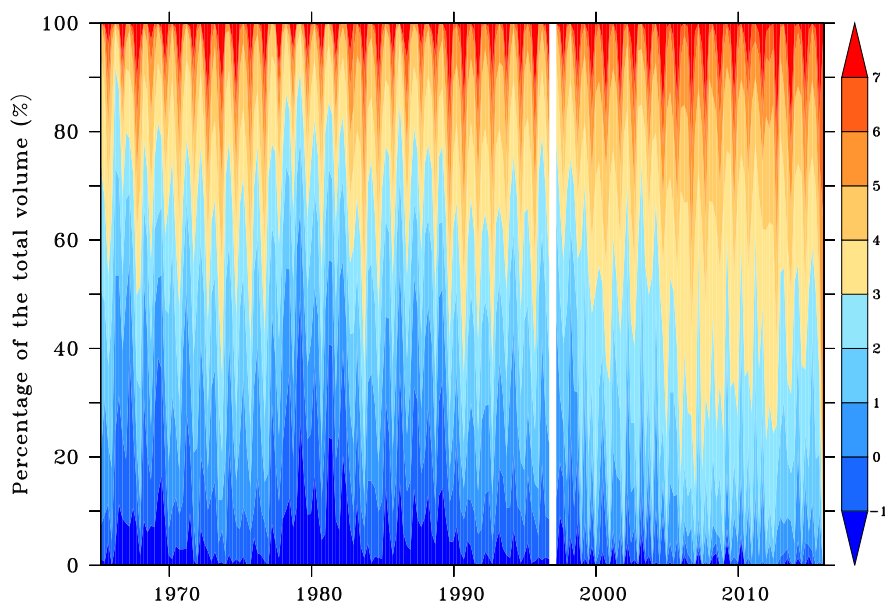
Figure 12. Volumetric temperature classes ranging from -1 to +7 °C in the Most Reliable Area between 1965–2015.
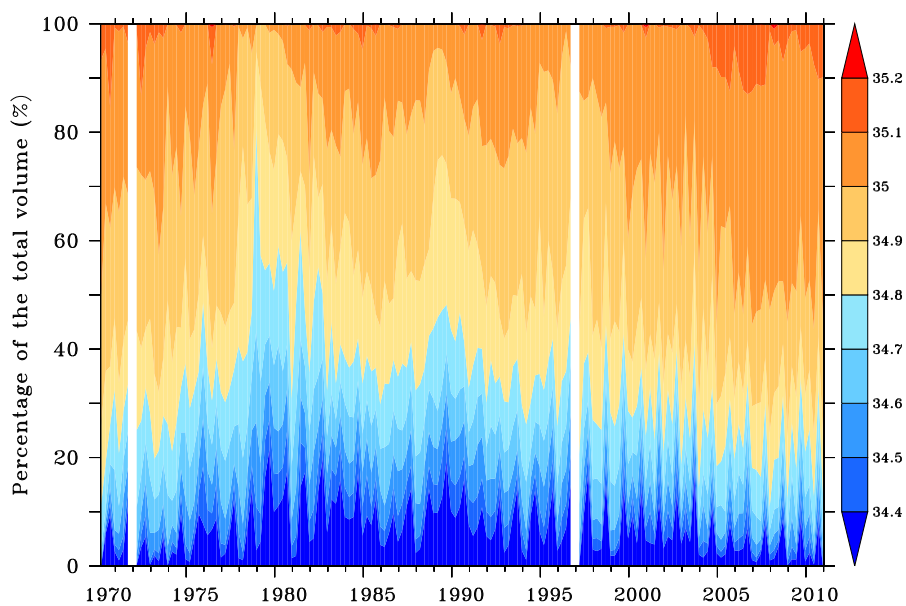
Figure 13. Volumetric salinity classes ranging from 34.4 to 35.2 PSU in the Most Reliable Area between 1970–2010.
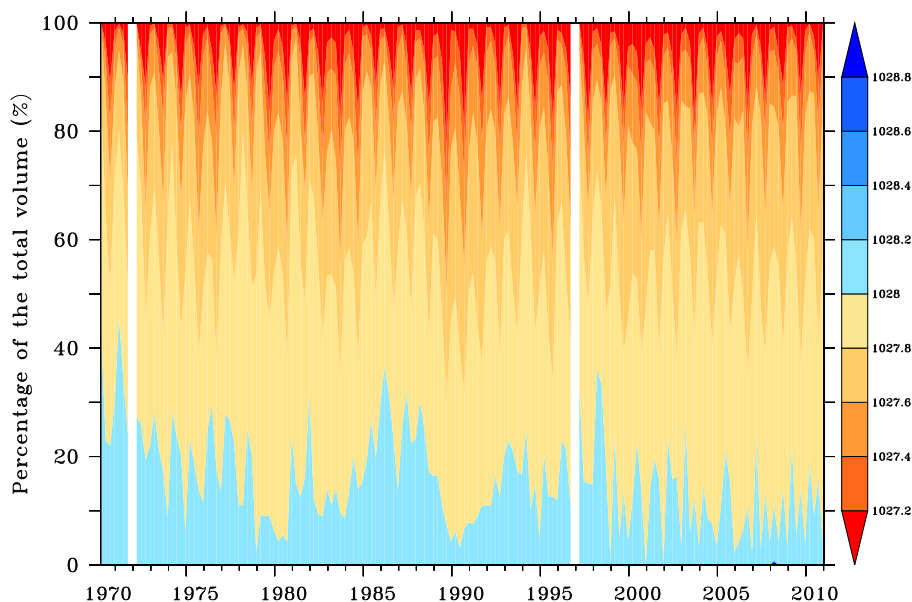
Figure 14. Volumetric potential density classes ranging from 1027.2 to 1028.8 $kg.m^{-3}$ in the Most Reliable Area between 1970–2010.

where t and s are temperature and salinity averages at each location between 1970–2010, ρ is the density of seawater, c_p is the specific heat of seawater taken here as 3985 $J\,kg^{-1}\,K^{-1}$ (Hill, 1962) and Δt is the temperature anomaly with respect to the reference period.

Fig. 15a shows the OHC changes in the MRA between 1965–2015. The time series shows a positive trend of 6.442×10^{16} $J.day^{-1}$ significant to the 95% level. The temperature from the BSO extracted from ICES (https://ocean.ices.dk/iroc/#) is also shown. The correlation between the temperature in the BSO and the OHC is 0.8921 (1976–2015), indicating that the temperature observed in the BSO is a reliable proxy for the OHC downstream in the southern part of the BS.

6.5 Equivalent freshwater content

To investigate changes in salinity in the MRA, we use the Boyer et al. (2007) definition of the Equivalent FreshWater Content (EFWC) to examine it.

$$EFWC = - \iiint \frac{\rho(t,s,p)}{\rho(t,0,p)} \frac{\Delta s}{s + \Delta s}\, dx\,dy\,dz \tag{2}$$

where Δs is the salinity anomaly with respect to the reference period 1970–2010.

In Fig. 15, the changes in EFWC in the MRA are shown between 1970–2010. The slope is -2.355×10^7 $m^3.day^{-1}$ with a R^2 of 0.1213, which means the negative trend is not significant at a confidence level of 95%, although very close to the threshold. For both OHC and EFWC trends significance, we followed the Fisher–Snedecor test described in Chouquet (2009) and Montgomery et al. (2012) augmented by a penalization of autocorrelation (Wilks, 1995). The salinity at the BSO extracted
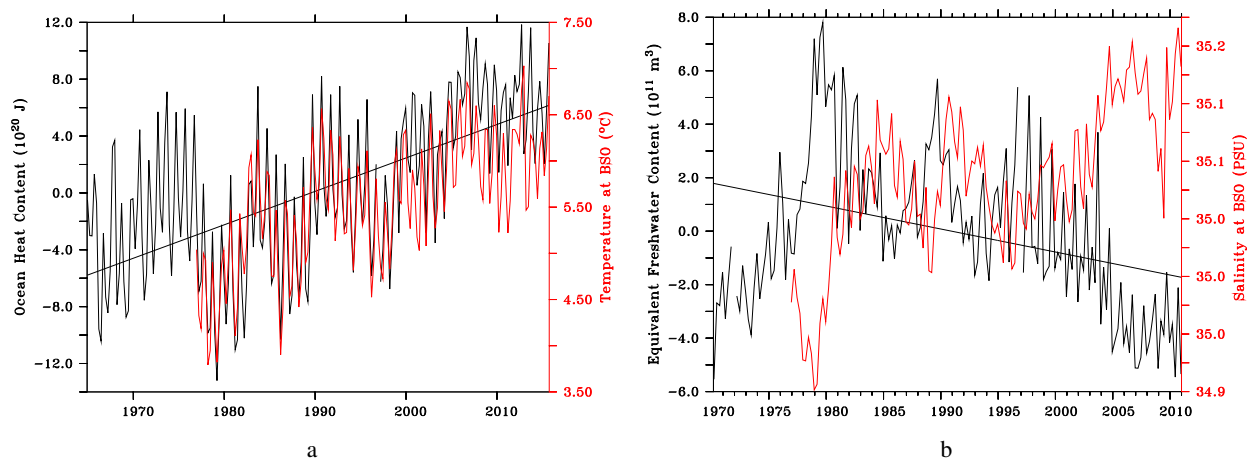
Figure 15. (a) Ocean heat content in the Most Reliable Area between 1965–2015, its linear trend (black) and temperature at the Barents Sea Opening. (b) Equivalent freshwater content in the Most Reliable Area between 1970–2010, its linear trend (black) and salinity at the Barents Sea Opening.

from ICES (https://ocean.ices.dk/iroc/#) is also shown. The correlation with the EFWC between winter 1976–1977 and winter 2010–2011 is -0.5628.

7 Conclusions

This research provides a comprehensive atlas of temperature and salinity covering the whole BS, with an emphasis on its MRA. Although the in–situ data is sometimes scarce on this part of the Arctic, we show here that much physical information can still be extracted from compiled databases provided a variational method minimising the expected errors on the resulting fields is used. The results are consistent with the recent "Atlantification" process of the BS already observed in the studies, i.e. a warmer and more saline BS, although only data from the autumn was included in the analysis on the whole BS. Using the MRA of the BS allows us to use a longer period (1965–2016) and to include all seasons in the analyses. This MRA exhibits similar results to the whole BS, with a positive trend in both temperature and salinity temperature and salinity, while no clear trend was found in density due to the cancelling effects of the increasing temperature and salinity on the density. This conclusion is supported by both vertical profiles and volumetric analysis. Finally, the computation of OHC and EFWC confirms these results as they show respectively positive and negative trend during 1965–2016. The measurements of temperature and salinity at the BSO are also consistent with the OHC and EFWC variabilities. The code as well as the data are made available online (see Sections 4 and 8) to encourage further research on this topic.

8   Code and data availability

The Diva software we used for this research as well as its user guide are available here: https://github.com/gher-ulg/DIVA. The data is accessible at https://doi.org/10.21335/NMDC-2058021735 (Watelet et al., 2020).

Author contributions.   Sylvain Watelet conducted the research and prepared the manuscript with contributions from all co-authors. Skagseth Øystein, Vidar Lien and Jean-Marie Beckers contributed in designing the research. Helge Sagen, Øivind Østensen, Vidar Lien helped preparing the data. Ivshin Viktor made possible the use of the Russian data. Jean-Marie Beckers helped with implementing DIVA.

Competing interests.   The authors declare that they have no conflict of interest.

Disclaimer.   The code is provided "as is", data quality as described by sources (e.g., WOD13). Diva is a software developed at the GeoHydrodynamic and Environmental Research (GHER, http://labos.ulg.ac.be/gher/) group at the University of Liège (https://www.uliege.be) and further developed for SeaDataNet scientific data products in JRA4 activities. Diva is copyright © 2006-2019 by the GHER group and is distributed under the terms of the GNU General Public License (GPL): http://www.gnu.org/copyleft/gpl.html

Acknowledgements.   The authors would like to thank the NPI for preparing data. The DIVA development has received funding from: the European Union Sixth Framework Programme (FP6/2002-2006) under grant agreement n° 026212, SeaDataNet, Seventh Framework Programme (FP7/2007-2013) under grant agreement n° 283607, SeaDataNet II, SeaDataCloud and EMODNet (MARE/2008/03 - Lot 3 Chemistry - SI2.531432) from the Directorate-General for Maritime Affairs and Fisheries.

References

Beckers, J.-M., Barth, A., Troupin, C., and Alvera-Azcárate, A.: Approximate and efficient methods to assess error fields in spatial gridding with data interpolating variational analysis (DIVA), Journal of Atmospheric and Oceanic Technology, 31, 515–530, 2014.

Boyer, T., Levitus, S., Antonov, J., Locarnini, R., Mishonov, A., Garcia, H., and Josey, S. A.: Changes in freshwater content in the North Atlantic Ocean 1955–2006, Geophysical Research Letters, 34, 2007.

Brasseur, P.: Reconstitution de champs d'observations océanographiques par le Modèle Variationnel Inverse: Méthodologie et Applications, Ph.D. thesis, Universite de Liege, Faculte des sciences appliquees, 1995.

Chouquet, C.: Modèles Linéaires, Laboratoire de Statistique et Probabilités, www.math.univ-toulouse.fr/~barthe/M1modlin/poly.pdf, [Online; accessed 22-September-2015], 2009.

Comiso, J. C. and Hall, D. K.: Climate trends in the Arctic as observed from space, Wiley Interdisciplinary Reviews: Climate Change, 5, 389–409, 2014.

Craven, P. and Wahba, G.: Smoothing noisy data with spline functions, Numerische mathematik, 31, 377–403, 1978.

Eriksen, E., Gjøsæter, H., Prozorkevich, D., Shamray, E., Dolgov, A., Skern-Mauritzen, M., Stiansen, J. E., Kovalev, Y., and Sunnanå, K.: From single species surveys towards monitoring of the Barents Sea ecosystem, Progress in Oceanography, 166, 4–14, 2018.

Fossheim, M., Primicerio, R., Johannesen, E., Ingvaldsen, R. B., Aschan, M. M., and Dolgov, A. V.: Recent warming leads to a rapid borealization of fish communities in the Arctic, Nature Climate Change, 5, 673–677, 2015.

Helland-Hansen, B. and Nansen, F.: The Norwegian Sea: its physical oceanography based upon the Norwegian researches 1900-1904, Det Mallingske Bogtrykkeri, 1909.

Hill, M. N. E.: The Sea: Composition of Sea-Water, vol. 2, Wiley, 1962.

Knipowitsch, N.: Hydrologische Untersuchungen im Europäischen Eismeer, Annalen der Hydrographie und Maritimen Meteorologie, 33, 241–260, 1905.

Kuhlbrodt, T., Rahmstorf, S., Zickfeld, K., Vikebø, F. B., Sundby, S., Hofmann, M., Link, P. M., Bondeau, A., Cramer, W., and Jaeger, C.: An integrated assessment of changes in the thermohaline circulation, Climatic Change, 96, 489–537, 2009.

Lind, S., Ingvaldsen, R. B., and Furevik, T.: Arctic warming hotspot in the northern Barents Sea linked to declining sea-ice import, Nature climate change, 8, 634, 2018.

Lozier, M., Li, F., Bacon, S., Bahr, F., Bower, A., Cunningham, S., De Jong, M., De Steur, L., Deyoung, B., Fischer, J., et al.: A sea change in our view of overturning in the subpolar North Atlantic, Science, 363, 516–521, 2019.

Mauritzen, C., Rudels, B., and Toole, J.: The Arctic and Subarctic Oceans/Seas, in: International Geophysics, vol. 103, pp. 443–470, Elsevier, 2013.

Montgomery, D. C., Peck, E. A., and Vining, G. G.: Introduction to linear regression analysis, vol. 821, John Wiley & Sons, 2012.

Reiniger, R. and Ross, C.: A method of interpolation with application to oceanographic data, in: Deep Sea Research and Oceanographic Abstracts, vol. 15, pp. 185–193, Elsevier, 1968.

Rixen, M., Beckers, J.-M., Brankart, J.-M., and Brasseur, P.: A numerically efficient data analysis method with error map generation, Ocean Modelling, 2, 45–60, 2000.

Schauer, U., Muench, R. D., Rudels, B., and Timokhov, L.: Impact of eastern Arctic shelf waters on the Nansen Basin intermediate layers, Journal of Geophysical Research: Oceans, 102, 3371–3382, 1997.

Swift, J. H., Takahashi, T., and Livingston, H. D.: The contribution of the Greenland and Barents seas to the deep water of the Arctic Ocean, Journal of Geophysical Research: Oceans, 88, 5981–5986, 1983.

Troupin, C., Barth, A., Sirjacobs, D., Ouberdous, M., Brankart, J.-M., Brasseur, P., Rixen, M., Alvera-Azcárate, A., Belounis, M., Capet, A., et al.: Generation of analysis and consistent error fields using the Data Interpolating Variational Analysis (DIVA), Ocean Modelling, 52, 90–101, 2012.

Watelet, S., Skagseth, Ø., Lien S., V., Sagen, H., Østensen, Ø., Ivshin, V., and Beckers, J.-M.: Barents Sea Atlas, NMDC, https://doi.org/10.21335/NMDC-2058021735, 2020.

Wilks, D. S.: Statistical methods in the atmospheric sciences, an introduction, vol. 59, Academic press, 1995.

Yang, X.-Y., Yuan, X., and Ting, M.: Dynamical link between the Barents–Kara sea ice and the Arctic Oscillation, Journal of Climate, 29, 5103–5122, 2016.